

Entropy-Slope Reconstruction from Late-Time Geometry in an MG-Unbiased Framework

Aiden B. Smith
Independent Researcher
(Dated: February 10, 2026)

We present a data-constrained reconstruction of the apparent-horizon entropy-slope function $\mu(A)$ from Pantheon+, cosmic chronometers, and BAO in a modified-gravity-unbiased late-time geometry framework. The primary posterior excludes GR-anchored growth, lensing, and full-shape closure inputs, so the entropy-sector inference is not pre-compressed by GR assumptions. For real data we find $\langle d\log \mu / d\log A \rangle = -0.237 \pm 0.315$, with $P(d\log \mu / d\log A > 0) = 0.214$, favoring negative slope. The same posterior gives $H_0 = 70.11_{-2.43}^{+2.47}$ km s $^{-1}$ Mpc $^{-1}$ and $\Omega_m = 0.297_{-0.043}^{+0.058}$. Mapping-systematic tests are subdominant to posterior width: fixed- Ω_m and residual variants shift median $\log \mu$ by at most 0.021 and 0.015, while the curved-horizon variant gives the largest shift, 0.056 (RMS significance 0.291 σ). Function-space distances disfavor strict BH ($D_{\text{BH}}^2 = 1.68 \times 10^{-4}$) relative to fitted non-BH families (best $D^2 = 4.54 \times 10^{-8}$). Synthetic BH-closure calibration with 24 simulation-based realizations yields near-nominal $\log \mu$ coverage (68%: 0.944; 95%: 1.000) and low invalid-logprob rate (1.00×10^{-3}). This provides a calibrated primary entropy-slope result for joint modified-gravity and Hubble-tension inference.

I. SCOPE

We reconstruct the horizon entropy-slope modifier

$$\mu(A) \equiv \frac{(dS/dA)_{\text{BH}}}{dS/dA}, \quad (1)$$

with the forward apparent-horizon mapping implemented in the entropy pipeline. We use the production configuration `entropy_submission_hardening_20260210_203502UTC`, including the real-data stage, robustness ablations, and synthetic closure calibration.

The real-data posterior uses the MG-unbiased profile: GR-anchored growth, lensing, and full-shape constraints are excluded from primary inference to reduce cross-sector GR-closure bias. Results therefore quantify the entropy slope required by late-time geometry channels under this mapping.

II. REAL-DATA RESULTS

A. Primary posterior

The real-data stage reports

$$H_0 = 70.11_{-2.43}^{+2.47} \text{ km s}^{-1}\text{Mpc}^{-1}, \quad (2)$$

$$\Omega_m = 0.297_{-0.043}^{+0.058}, \quad (3)$$

with acceptance fraction 0.337 and minimum effective sample size $\text{ESS}_{\min} \approx 3995$.

The entropy-slope summaries are

$$\left\langle \frac{d \log \mu}{d \log A} \right\rangle = -0.23697 \pm 0.31483, \quad (4)$$

$$P\left(\frac{d \log \mu}{d \log A} > 0\right) = 0.2143, \quad (5)$$

so $\sim 78.6\%$ posterior weight lies at negative slope. The area-averaged offset statistic is consistent with small net displacement,

$$\langle m \rangle = -0.0035 \pm 0.1523. \quad (6)$$

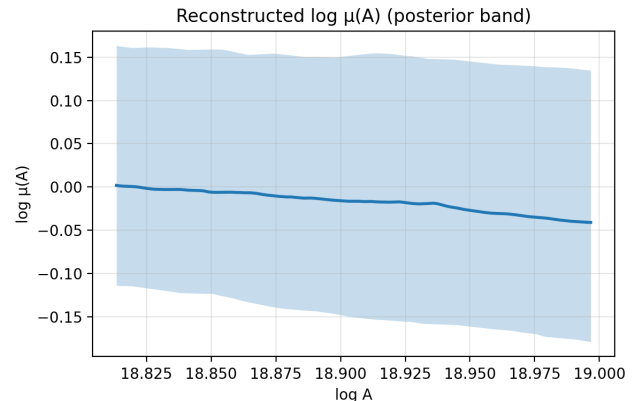


FIG. 1. Posterior band for $\log \mu(\log A)$ from the finalized MG-unbiased real-data stage.

B. Mapping-variant robustness

Mapping stress tests are stable relative to posterior width. Relative to the baseline variant (V1_free), median-shape shifts are:

- V0_fixedOm: $\text{RMS}(\Delta \mu / \sigma) = 0.080$, $\max |\Delta \log \mu| = 0.0214$.
- V2_residual: $\text{RMS}(\Delta \mu / \sigma) = 0.062$, $\max |\Delta \log \mu| = 0.0153$.
- V1_curved: $\text{RMS}(\Delta \mu / \sigma) = 0.291$, $\max |\Delta \log \mu| = 0.0562$.

The curved-horizon nuisance is the dominant mapping perturbation but remains sub- 1σ in RMS significance.

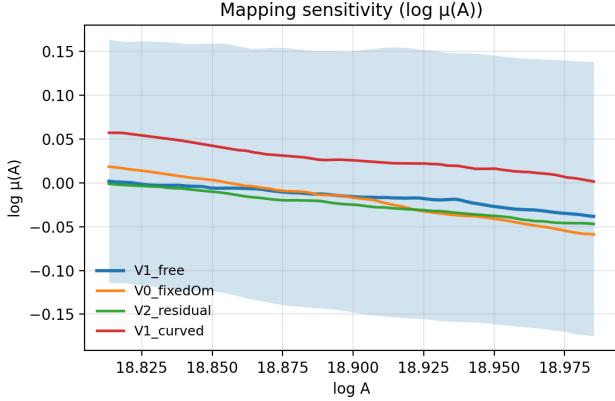


FIG. 2. Mapping-variant comparison of reconstructed $\log \mu(\log A)$.

C. Function-space proximity

Weighted function-space distances to parametric families (fit to posterior mean) are

$$\begin{aligned} D_{\text{BH}}^2 &= 1.68 \times 10^{-4}, \\ D_{\text{Tsallis}}^2 &= 4.54 \times 10^{-8}, \quad D_{\text{Barrow}}^2 = 4.54 \times 10^{-8}, \\ D_{\text{Kaniadakis}}^2 &= 1.12 \times 10^{-7}. \end{aligned} \quad (7)$$

In this run, non-BH families track the reconstructed shape much better than strict BH. Best-fit summary parameters are $\delta_{\text{Tsallis}} = 1.23697$, $\Delta_{\text{Barrow}} = 0.47393$, and $\beta_{\text{Kaniadakis}} = 0.50660$.

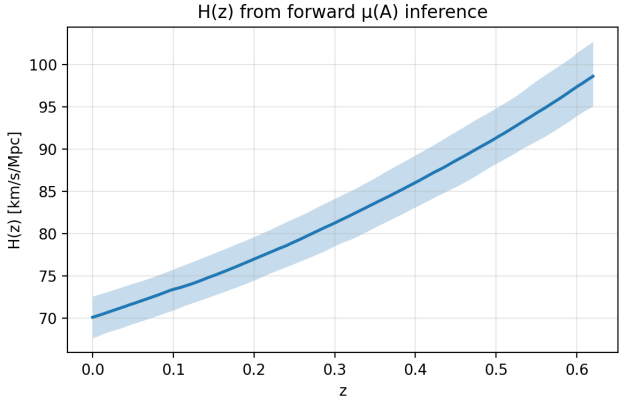


FIG. 3. Forward-reconstructed $H(z)$ band for the same posterior draws.

III. ABLATION AND SYNTHETIC CLOSURE

A. Ablation suite

Seven ablation cases were executed (kernel, covariance,

and smoothing variations). Across cases,

$$D_{\text{BH}}^2 \in [0.117, 0.553], \quad \min D_{\text{Kaniadakis}}^2 = 4.37 \times 10^{-3}. \quad (8)$$

The qualitative ordering is consistent with the real-data stage: non-BH families remain much closer than BH across tested settings.

B. Synthetic BH closure (SBC)

The synthetic closure stage completed $N = 24$ SBC realizations with BH truth. Coverage metrics are

$$\log \mu(x) : C_{68} = 0.944, C_{95} = 1.000, \quad (9)$$

$$\log \mu(\log A) : C_{68} = 0.940, C_{95} = 1.000, \quad (10)$$

$$H(z) \text{ pointwise} : C_{68} = 0.739, C_{95} = 0.981, \quad (11)$$

$$H(z) \text{ simultaneous} : C_{68} = 0.917, C_{95} = 0.958. \quad (12)$$

Sampler health remained stable. SBC acceptance was 0.3628 on average ($p10/p50/p90 = 0.3589/0.3625/0.3693$). The invalid-logprob rate was 1.00×10^{-3} ($p90 1.53 \times 10^{-3}$; max 1.80×10^{-3}), dominated by prior-bound hits on $\log \sigma_{d2}$.

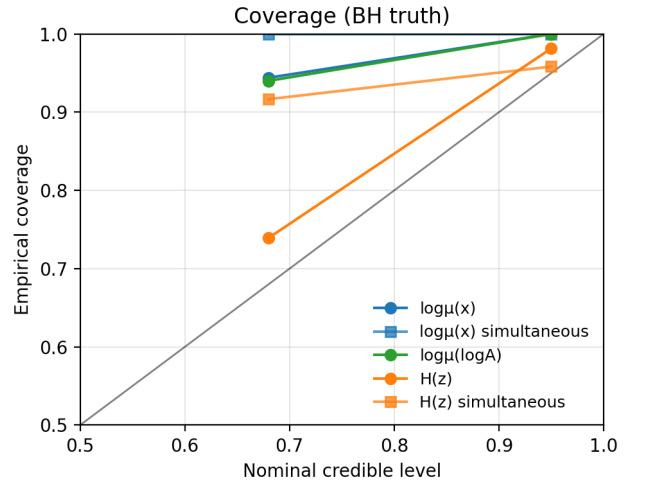


Figure: Synthetic-closure coverage summary from the BH-truth SBC stage.

IV. CONCLUSION

This work delivers a standalone entropy-slope measurement from MG-unbiased late-time geometry. The posterior favors negative slope with broad but finite uncertainty; mapping-variant shifts remain subdominant; and function-space tests prefer non-BH families over strict BH for the recovered profile. Synthetic closure calibration indicates numerically stable, near-nominal coverage behavior. Taken together, these results define a calibrated entropy-sector constraint that can be propagated directly into joint modified-gravity and Hubble-tension analyses.

ACKNOWLEDGMENTS

85

This work used A.I. tools extensively, including ChatGPT 5.3.

75 **DATA AVAILABILITY AND DOIS**

90

- O3 modified-gravity tension anomaly repository (Zenodo): <https://doi.org/10.5281/zenodo.18603134>.
- O3 search-sensitivity injection data (Zenodo): <https://doi.org/10.5281/zenodo.7890437>.
80
- GWTC-3 catalog: <https://doi.org/10.1103/PhysRevX.13.041039>.
- Pantheon+ constraints: <https://doi.org/10.3100847/1538-4357/ac8e04>.
85

- Planck 2018 parameters: <https://doi.org/10.1051/0004-6361/201833910>.
- Planck 2018 lensing: <https://doi.org/10.1051/0004-6361/201833886>.
- SDSS DR12 BAO: <https://doi.org/10.1093/mnras/stx721>.
- eBOSS DR16 constraints: <https://doi.org/10.1103/PhysRevD.103.083533>.
- DESI 2024 BAO constraints: <https://doi.org/10.1088/1475-7516/2025/02/021>.
- Cosmic-chronometer component DOI: <https://doi.org/10.1088/1475-7516/2012/08/006>.
- Cosmic-chronometer component DOI: <https://doi.org/10.1103/PhysRevD.71.123001>.
- Cosmic-chronometer component DOI: <https://doi.org/10.1088/1475-7516/2010/02/008>.